The Effect of Welding on the Breakdown and Repassivation Potentials of Alloy 22 in 5 M CaC1$_2$

G.O. Ilevbare

August 28, 2003

U.S. Department of Energy

Lawrence
Livermore
National
Laboratory

This report has been reproduced directly from the best available copy.

Available electronically at http://www.doc.gov/bridge

Available for a processing fee to U.S. Department of Energy
And its contractors in paper from
U.S. Department of Energy
Office of Scientific and Technical Information
P.O. Box 62
Oak Ridge, TN 37831-0062
Telephone: (865) 576-8401
Facsimile: (865) 576-5728
E-mail: reports@adonis.osti.gov

Available for the sale to the public from
U.S. Department of Commerce
National Technical Information Service
5285 Port Royal Road
Springfield, VA 22161
Telephone: (800) 553-6847
Facsimile: (703) 605-6900
E-mail: orders@ntis.fedworld.gov
Online ordering: http://www.ntis.gov/ordering.htm

OR

Lawrence Livermore National Laboratory
Technical Information Department's Digital Library
http://www.llnl.gov/tid/Library.html

THE EFFECT OF WELDING ON THE BREAKDOWN AND REPASSIVATION POTENTIALS OF ALLOY 22 IN 5 M CaCl$_2$

G. O. Ilevbare
Lawrence Livermore National Laboratory
7000 East Ave, L-631, Livermore CA 94550, USA

ABSTRACT

The study of the electrochemical behavior of wrought and welded Alloy 22 was carried out in 5 M CaCl$_2$ between 45 and 120 ^{o}C with Multiple Crevice Assembly (MCA) specimens. The susceptibility to corrosion was found to increase with increase in temperature in both the wrought and the welded forms of the alloy. The weld metal was found to be less susceptible to localized corrosion under the conditions tested.

INTRODUCTION

Alloy 22 (UNS number N06022) is a nickel alloy rich in chromium and molybdenum, with a high degree of corrosion resistance. It exhibits a low general corrosion rate under most conditions and has formidable localized corrosion resistance in most environments compared with other nickel alloys [1-8]. Alloy 22 is the candidate material for the fabrication of high-level nuclear waste containers. These containers are intended for use for disposal of high-level radioactive waste and spent nuclear fuel. On July 23, 2002, The United States Congress approved the site at Yucca Mountain, Nevada, for development as a repository for disposal of nuclear waste.

Since welding will be used to close the waste containers, it is important to fully characterize and understand the electrochemical behavior of the welds and the areas adjoining the welds. One method of comparison is to characterize the behavior of non-welded (wrought) and welded Alloy 22 to determine whether there is increased susceptibility to corrosion in the welded zones and areas adjacent to the welded zones.

The study of the effect of temperature on the corrosion properties of the alloy is important since during the projected 10,000-year service life, the containers will pass through a heat gradient caused by the heat generated from radioactive decay. Temperatures will be high (above the boiling point of water) in the early service life of the containers, while lower temperatures will prevail much later due to decreased radioactive decay. At this later stage, there is an increased possibility of ground water contacting the containers.

A range of water chemistries is expected to be in contact with the waste containers during its service live. The effect of important individual anions (like Cl$^-$), which could impact the performance of the containers, must be understood. Crevice corrosion is a concern in Cl$^-$ environments [2-4]. Consequently, the study of the crevice corrosion behavior of

Alloy 22 in the wrought and welded forms has been carried out in 5 M $CaCl_2$ using a multiple crevice assembly (MCA) sample configuration. This configuration was optimized for the study of crevice corrosion as it provides 24 potential crevice generation sites on a surface area of less than 10 cm^2. The temperature range of study was between 45 and 120 ^{o}C (± 2 ^{o}C).

EXPERIMENTAL PROCEDURE

The material used in this study is Alloy 22 (N06022). Alloy 22 samples were fabricated from wrought and welded plate specimens. The chemical composition as documented by the supplier appears in Table 1. The composition is consistent with ASTM-B 575 (for plates/sheets) standard [9, 10]. The wrought samples were made out of flat sheets that were ~2 mm thick, while the welded samples were made from plates that were 3.175 cm (1.25 inch) thick. The composition of the filler metal was taken before it was used in the welding process. The Multiple Crevice Assembly (MCA) specimens look like lollipops (Figure 1). The design was optimized for the study of crevice corrosion so that most of the working surface was covered by the ceramic crevice former. The working surfaces of the MCA samples were used in the as-received state after degreasing with acetone and methanol. In the as-received state, the working surfaces of the MCA samples were finished to a root mean square (RMS) roughness average (RA) of between 2 and 5 micro inches with an air formed oxide film. The edge (surface 90 degrees in angle to the working surface) of the samples was finished with 600-grit SiC paper after first grinding with 100 and then 240-grit paper to remove damage done to them by the electric discharge machine (EDM) used during fabrication. The welded MCA specimens were identical to the wrought specimens in configuration. The welds were made by means of Gas Tungsten Arc Welding (GTAW). The double-U shaped welds were completed in about 8-10 passes (Figure 2). The weld metal on the welded samples was taken from the outermost portion (surface) of the welds. Since the welds had a double-U configuration, this meant that the volume of weld metal on the sample was not the same throughout the ~2 mm thickness of the samples. Nonetheless, the amount of weld metal on the samples covered an area on the working surface that was at least 1 cm wide and extended across the entire face (perpendicular to the stem of the sample) of the specimen on which the crevice formers were assembled. The rest of the MCA consisted of Titanium (Ti) grade 2 nuts, bolts and washers, as well as ceramic crevice formers with multiple ridges. The bolts were polytetrafluoroethylene (PTFE) wrapped to prevent these hardware components from being in electrical contact with the specimen. Each crevice former had a total of 12 ridges on it, creating 12 different potential crevice sites on each face of the specimen, and a total of 24 potential sites in each assembly (Figure 1). The assembly was tightened to a torque of 70 in-lb. PTFE tape inserts were placed between the ceramic crevice former and the MCA sample prior to tightening. This was done to fill in the micro voids created by the micro-rough surfaces of the sample and the ceramic crevice former, and to increase the reproducibly of the tight crevices in all samples. The total surface area of the MCA specimen immersed in the electrolyte was 7.43 cm^2. This surface area included the area under the 24 ridges of the crevice formers, which had a combined surface area of 1.6 cm^2. In current density estimations, the surface area of 7.43 cm^2 was used for calculations.

A three-electrode cell with a capacity of 1000 cm^3 was used for experimentation. The volume of electrolyte in the cell was ~900 cm^3. A saturated silver/silver chloride (SSC) (Ag/AgCl) electrode was the reference electrode (RE). The RE was maintained near room temperature by mounting it at the end of a Luggin probe, which had a water-cooled jacket around it. The temperature of the water pumped through the cooling jacket was between 5 and 12 ^{o}C. Thermal liquid junction calculations showed that potential variation caused by this phenomenon was in the order of a few mV (~10 mV maximum). Also, according to Macdonald et al., a high KCl concentration in the reference electrode tends to suppress thermal liquid junction potentials across the boundary between the high and low temperature solutions [11]. The liquid junction potential variations were therefore ignored in further analyses. The counter electrode was made of platinum (Pt) foil. The temperature of the electrolyte was maintained by means of an oil-filled heating bath. The sample was immersed into the cell after the electrolyte had attained the desired temperature. This was done immediately after the grinding process. The temperature was taken before and after the experiment with a thermocouple immersed into the electrolyte. Electrochemical measurements were carried out using a potentiostat. The corrosion potential (E_{corr}) was monitored for 24 hours. This was followed by cyclic potentiodynamic polarization measurements immediately afterwards. Cyclic polarization was started approximately 100 mV below E_{corr}, and continued until the current density from the sample reached a maximum of up to 30 mAcm^{-2}, or a maximum of 1.3 V (SSC) before the scan was reversed. An upper limit of 30 mAcm^{-2} was chosen to facilitate the observation of any anodic peaks that might occur (and repassivate) with current densities as high as 20-30 mAcm^{-2} generated (especially at 75 ^{o}C) on Alloy 22 in 5 M CaCl$_2$. The sweep rate in the forward and reverse directions was 0.1667 mVs^{-1} (600 mVh^{-1}). Deaerated 5 M CaCl$_2$ with a pH~5 was used, at various temperatures in these experiments. Nitrogen gas (N$_2$) was bubbled through the electrolytes for at least one hour before and throughout the experiments at a rate of ~100 cc per minute. All electrolytes were prepared using certified American Chemical Society (ACS) reagent grade chemicals. In other experiments, potentiostatic polarization experiments were carried out for up to 24 hours in the same three-electrode configuration cell immediately after the 24-hour corrosion potential (E_{corr}) monitoring period.

EXPERIMENTAL RESULTS

The Corrosion Potential (E_{corr})

Figure 3 shows a summary of the average E_{corr} values between 45 ^{o}C and 120 ^{o}C for wrought and welded samples of Alloy 22. The number of repeats which make the average values presented range from 3 to 6. The error bars in Figure 3 are the standard deviations of the distributions. In each experiment, E_{corr} was recorded at the end of the 24-hour period of the experiments and used to compute the averages shown. Figure 3 shows that E_{corr} from the wrought and welded specimens can only be separated with confidence at 45 and 90 ^{o}C. They are statistically similar at all other temperatures as indicated by the overlapping of the error bars. The E_{corr} of the wrought samples was not affected by temperature. The difference between the highest and lowest mean values of E_{corr} between 45 and 120 ^{o}C was ~20 mV. However, the welded samples were affected by temperature. The E_{corr} of welded samples decreased with increase in temperature.

There was a difference of ~120 mV between the highest and lowest mean E_{corr} values recorded on the welded samples. Nonetheless, the E_{corr} values for the wrought and welded metals were relatively close over the entire range of temperature considered in these measurements (Figure 3).

The Breakdown Potential (E_b)

The critical breakdown potential, E_b, as employed here is used to denote the potential(s) at which the breakdown of the passive film occurs by any type of corrosion attack such as pitting corrosion, crevice corrosion, general dissolution, or transpassive dissolution.

Figures 4 and 5 show representative polarization curves at the extremes of the temperature range tested (45 and 120 ^{o}C) for the wrought and welded MCA samples. At 45 ^{o}C, the curves for both the wrought and the welded forms of Alloy 22 showed a similar behavior, and overlap almost exactly. Localized breakdown due to crevice corrosion did not occur on any of the samples tested at this temperature on both the wrought and the welded samples. At 120 ^{o}C (Figure 5), the polarization curves of wrought and welded Alloy 22 were also similar. However, the welded sample exhibited a higher breakdown potential compared with the wrought sample. The polarization curves of the wrought at 60, 75 and 90 ^{o}C were similar to those collected from the welded samples at the corresponding temperatures. The polarization curves at 90 ^{o}C were similar to those at 120 ^{o}C. At 60 and 75 ^{o}C however, the shape of the curves, and thus the electrochemical behavior of Alloy 22 differed from those at 90 and 120 ^{o}C (Figure 6). In Figure 6, there is a drop in current density after an initial rise in current density from the passive region at 60 and 75 ^{o}C. This drop in current density created an "anodic peak" or "hump" usually between 0.0 and 0.5 V_{SSC}, however, broader peaks have occurred on samples at 75 ^{o}C. The peaks at 75 ^{o}C are broader and have higher peak current densities than those at 60 ^{o}C. These current excursions could sometimes reach values of about 20-30 mAcm^{-2} at 75°C. After the anodic peak or hump, there is a secondary passive region. The current density of the secondary passive region was higher than that of the primary passive region. The current density of the secondary passive region at 75 ^{o}C was much greater than that at 60°C. Beyond the secondary passive region, transpassive dissolution results on further increase of the applied potential. Localized corrosion was observed on samples (at 60 ^{o}C) where the potential was reversed at or near the peak current density in the anodic peak after inspection with an optical microscope. At 60 and 75 ^{o}C where the experiments proceeded to potentials corresponding to regions of transpassive dissolution, two types of damage were observed on the sample, localized corrosion, which occurred at potentials corresponding to the anodic peak or hump, and general dissolution due to transpassivation, which occurred at much higher potentials. As observed in Figure 6, no hystereses loop occurs (at 60 nor 75 ^{o}C) when the potential is taken to the transpassive region. Samples where the applied potential was reversed in the anodic peak did not exhibit any generalized dissolution. Not all the wrought samples tested at 60 ^{o}C (and none of the 3 welded samples tested at 60 ^{o}C) exhibited the hump. Only transpassive dissolution occurred at higher potentials at 60 and 75 ^{o}C, consistent with the absence of hystereses loops at these elevated potentials. The reason for this behavior is not fully understood.

Figure 7 shows a summary of the breakdown potentials (E_b) and the repassivation potential E_{rp} for both the wrought and the welded samples. These data points are from an average of at least 2 data values. The error bars are standard deviations of the distribution. E_{corr} values have been included for easy comparison with E_b and E_{rp}. The method used to determine E_b was the current density inflection (of the curve) method. In this method, E_b is the potential at which a permanent rise in current density from the passive region commences. In most cases, E_b was easily determined due to the abrupt increase in current indicative of the onset of localized breakdown (Figure 5). At 60 and 75 °C where anodic peaks or "humps" occur, E_b was taken as the base of the "hump". Samples held at a potential (~0.325 V_{SSC}) corresponding to the peak current density in the hump at 75 °C (Figure 6) in potentiostatic polarization experiments for up to 24 hours showed that the samples did not passivate. In fact, there was massive dissolution of the metal, hence the potential at the base, where the current density started to rise, was taken as E_b. Figure 8 shows about 70,000 s of the current and current density transients from a potentiostatic experiment performed at 75 °C. The abrupt fall in current and current density at about 67 000s possibly coincides with the detachment of the lollipop head from the stem of the sample (refer to Figure 1).

E_b decreased steadily with increase in temperature between 45 and 120 °C (Figure 7). At 45 °C, on both the wrought and the welded samples, E_b was due to transpassive dissolution and not localized breakdown. This was also true at 60 °C on the welded samples. At 75 °C and above, E_b represented localized breakdown on both the wrought and welded samples. E_b at 75 and 90 °C were difficult to separate statistically since the error bars overlapped. However, at 120 °C, E_b was higher on the welded samples, and hence more resistant to localized corrosion compared with the wrought samples.

The degree of damage due to localized corrosion increased with increasing temperature. The crevices formed at 60 °C were the shallowest and caused the least damage per unit area. Crevice corrosion was virtually non-existent in the weld metal zone in welded samples (Figures 9 and 10). Where it occurred, it was less severe than in the crevices of the base metal zone. In Figure 9 (75 °C; 5 M $CaCl_2$), the band of weld metal appears darker than the base metal zone in the top portion of the photo. The deepest crevices are located in the base metal zone. Similarly, in Figure 10 (120 °C, 5 M $CaCl_2$), the deep crevices that formed in the lower base metal half of the image seem to terminate at the boundary of the base and weld metal. In Figure 10, the weld metal zone seems to deflect the growth path of the crevices away from itself, thus confining it to the base metal zone. These images suggest that the weld metal is significantly better able to resist localized attack in 5 M $CaCl_2$ in spite of the similarities in the E_b of the wrought and welded samples especially at 75 and 90 °C.

The Repassivation Potential (E_{rp})

Two methods were used to measure the repassivation potential for localized corrosion, E_{rp}. In the first method, the repassivation potential was taken as the potential that coincided with a current density of 1 μAcm^{-2} (1 x 10^{-6} Acm^{-2}) on the reverse sweep of the cyclic polarization curves. "E_{rp1}" in Figure 7 denotes the values obtained in this fashion. In the second method, denoted by "E_{rp2}" (Figure 7), the repassivation potential was the potential that coincided with the point at which the reverse and forward sweeps of the

polarization curve intersected. Figure 7 shows that comparable values of E_{rp} are obtained from the two methods, as exemplified in the similarities of E_{rp1} and E_{rp2}. In fact, at 75, 90 and 120 °C, the values were statistically indistinguishable because of the overlap of the error bars. There are no E_{rp} values for the wrought and welded samples at 45 °C, and for the welded samples at 60 °C since there was no localized corrosion on the samples at these temperatures. Although localized corrosion was observed on the wrought samples at 60 °C, and on both the wrought and welded samples at 75 °C, the E_{rp} values assigned to Alloy 22 at these temperatures might not be the true E_{rp} values. This is because the damage sustained by these samples under the said conditions at the time of applied potential reversal was not localized corrosion, but rather transpassive dissolution (Figure 6). More accurate E_{rp} values would be obtained by reversing the potential in the region where localized corrosion is active, that is, by the peak current density in the "hump". There is a difference of at least 240 mV$_{SSC}$ between E_b and E_{rp} in the wrought and the welded samples, with E_{rp} being the lower potential as expected. E_{rp} decreased with increasing temperature, just as E_b did. The E_{rp} values were similar for both the wrought and the welded samples, even at 120 °C where E_b was different. All E_{rp} values were higher than the corresponding E_{corr} values (Figure 7). That is, to attain localized corrosion, of Alloy 22 in pure 5 M CaCl$_2$ solution, polarization above E_{corr} is required.

DISCUSSION

A range of water compositions is expected to contact the waste containers at Yucca Mountain [12]. Understanding the effect of Cl$^-$ on the corrosion process is important for evaluating these environments. Hence, high Cl$^-$ only environments (5 M CaCl$_2$ (10 M Cl$^-$)) were evaluated in this study. It should be noted that waters sampled at Yucca Mountain contain an array of anions and oxyanions, which include NO$_3^-$ and SO$_4^{2-}$, which have been found to inhibit localized corrosion in stainless steels and nickel alloys [13-22]. Indeed, earlier work showed that Alloy 22 is not susceptible to localized corrosion in simulated concentrated multi-ionic solutions [1].

The similarity in the values of the E_{corr} (except at 45 and 90 °C) for the wrought and the welded samples over the temperature range tested suggest that there might be difficulty in creating and sustaining viable galvanic couples which could lead to localized breakdown of the oxide film either on the base metal or weld (depending on which potential is higher). A possible reason for this is because the composition for the weld metal in the welded sample is similar to that of the base metal (Table 1). In addition, the E_{corr} values recorded for the welded specimens are in reality, a composite of the welded and wrought materials.

A limitation of the method used in the determination of E_b is that it is not able to give the exact potential at which localized breakdown commences. This is because the current values being monitored for localized corrosion are composites of the passive current density and that due to localized corrosion. Therefore, in order for a current rise (over and above the passive (background) current) to be observed, the localized corrosion event would need to grow to such as size that would enable it to put out a current higher than that of the passive current of the specimen. The amount of growth that is required would depend on how large the surface of the specimen is since it scales directly with the value

of the background current. Generally, the smaller the sample, the earlier the current due to localized breakdown will be detected, and the closer the determined E_b will be to the actual potential at which localized breakdown commenced [23]. However, increasingly smaller samples might lead to elevated E_b values, as the number of potential sites for the nucleation of localized events reduces with size. Other methods like the current threshold method, in which a current or current density is used to determine the onset of localized corrosion is also froth with uncertainties with regard to determining the exact onset of localized corrosion. Too low a threshold current value will lead to E_b values in the regions where the sample is still passive. Too high a threshold value leads to E_b values that are too high. Hence, the current threshold method is best employed only as a basis for comparison amongst systems.

The similar values of E_b obtained at 75 and 90 ^{o}C, and higher values obtained at 120 ^{o}C for the wrought and welded samples of Alloy 22 in 5 M $CaCl_2$ suggest that in this environment, GTAW welds did not cause any adverse effect on the resistance of Alloy 22 to localized corrosion under the present test conditions. The images in Figure 9 and 10 suggest that the weld and base metal exhibit different propensities to crevice corrosion, with the weld metal able to better resist crevice corrosion. Since the welded samples do not contain pure weld metal, the values of E_b presented for both the welded and wrought samples might therefore reflect the E_b of the wrought or base metal, rather than that of the weld metal alone. Since the closeness of the E_{corr} values between the wrought and the welded samples suggest that powerful galvanic couples may not be viable, or easy to sustain, the greater susceptibility of the base compared with the weld metal is believed to be due to a metallurgical effect. However, the fact that both weld and base metal are present on the same sample creates a difficulty in accurately acquiring the contribution of each metal type to the E_{corr} of the welded MCA samples. Nonetheless, although the E_{corr} of the welded sample is a composite of the E_{corr} of the weld and base metals, the closeness of the E_{corr} of the wrought and welded samples strongly suggests that the E_{corr} of pure base metal (wrought) might be close to that of pure weld metal. Clearly, more work is required in this area to understand, and possibly isolate the main reason(s) for the differences in susceptibility to localized corrosion.

The anodic peaks or "humps" exhibited by both the wrought and the welded versions of the sample at 60, and 75 ^{o}C are associated with localized attack that passivated upon increase in potential. In addition, there is some difficulty in reactivating the sites of localized breakdown after passivation has occurred. The reason why passivation took place after initial breakdown is not fully understood. However, potentiostatic polarization experiments carried out at potentials equivalent to the maximum current density in the anodic peak showed that high current densities required to sustain metal dissolution were sustained throughout the experiment (Figure 8), despite of the slight fall in these current densities with time.

CONCLUSIONS

1.   After 24 hours of exposure to 5 M $CaCl_2$, the E_{corr} of the wrought MCA Alloy 22 is not affected by temperature between 45 and 120°C. However, after 24 hours of exposure to 5 M $CaCl_2$, the E_{corr} of the welded MCA samples of

Alloy 22 decreases ~120mV with increase in temperature between 45 and 120 $^{\circ}$C.

2. During anodic potentiodynamic polarization, localized corrosion was observed on wrought samples of at 60 $^{\circ}$C and above, and at 75 $^{\circ}$C and above for the wrought and welded samples respectively in 5 M $CaCl_2$. No localized corrosion was observed at 45 $^{\circ}$C on both the wrought and welded samples, and at 60 $^{\circ}$C on the welded samples in 5 M $CaCl_2$.

3. E_b shifted to lower potentials as temperature increased on both the wrought and welded samples in 5 M $CaCl_2$.

4. E_b was similar on the wrought and welded samples at 75 and 90°C but was lower on the wrought samples at 120 $^{\circ}$C in 5 M $CaCl_2$.

5. The weld metal was found to be less susceptible to crevice attack compared with the base metal in the welded samples in 5 M $CaCl_2$.

6. Where localized corrosion occurred, the E_{rp} was similar on both the wrought and the welded samples in 5 M $CaCl_2$.

7. E_{rp} decreased with increase in temperature on the wrought and welded samples in 5 M $CaCl_2$.

REFERENCES

1. G.O. Ilevbare T. Lian and J.C. Farmer, Environmental Considerations in the Studies of Corrosion Resistant Alloys for High-Level Radioactive Waste Containment Paper No. 02539, Corrosion 2002.

2. G.O. Ilevbare, Electrochemical Behavior of Alloy 22 in 5 M $CaCl_2$, Transportation Storage, and Disposal of Radioactive Materials, PVP-Vol. 449, p.55 2002. American Society of Mechanical Engineers (ASME), New York, USA.

3. B. A. Kehler, G.O. Ilevbare and J.R. Scully Corrosion, 57, pp. 1042, 2001.

4. B. A. Kehler, G. O. Ilevbare and J. R. Scully Corrosion 2001, Crevice Corrosion Behavior, of Ni-Cr-Mo Alloys: Comparison of Alloys 625 and 22, NACE Topical Research Symposium, p.30, March 2001.

5. Haynes International, Inc., Product Brochure H-2019E, Haynes International Inc. Kokomo, IN, p.22, 1997.

6. J. C. Farmer, D. McCright, G.E. Gdowski, F. Fang, T. Summers, P. Bedrossian, J. Horn, T. Lian, J. Estill, A. Lingenfelter, and W. Halsey, General and Localized Corrosion of Outer Barrier of High-Level Waste Container in Yucca Mountain, May 2000. Preprint UCRL-JC-138890, Lawrence Livermore National Laboratory, Technical Information Department Digital Library.

7. K.A. Gruss, G.A. Cragnolino, D.S. Dunn and N.Sridhar, Corrosion '98, Paper No. 149, 1998.

8. S.J. Lukezich, The Corrosion Behavior of Ni-Base High Performance Alloys in Simulated Repository Environments, MS Thesis, The Ohio State University 1989.

9. ASTM B574, Annual Book of ASTM Standards, Nonferrous Metal Products, Volume 02.04, p.531, American Society of Testing and Materials, West Conshohocken, PA (2000).

10. ASTM B575, Annual Book of ASTM Standards, Nonferrous Metal Products, Volume 02.04, p.535, American Society of Testing and Materials, West Conshohocken, PA (2000).
11. D.D. Macdonald, A.C. Scott, and P. Wentrcek, J. Electrochem. Soc., **126**, 908 (1978).
12. N.D. Rosenberg, G.E. Gdowski, and K.G. Knauss, Applied Geochemistry, 2001. **16**: p.1231.
13. R.C. Newman and T. Shahrabi, Corrosion Science, 1987. **27**: p.827.
14. H. Yashiro and K. Tanno, Corrosion Science, 1990. **31**: p. 485.
15. H.H Uhlig and J.R. Gilman, Corrosion, **20**, 289t (1964).
16. H. P. Leckie and H.H. Uhlig, J. Electrochem. Soc., **117**, 1152 (1966).
17. I.L. Rozenfeld, and I.S Danilov, Corrosion Science, **7**, 129 (1967).
18. E.A. Lizlovs and A.P. Bond, J. Electrochem Soc., **116**, 574 (1969).
19. Z. Szklarska-Smialowska, Corrosion Science, **11**, 209 (1971).
20. Z. Ahmed, Corrosion, **33**, 161 (1977).
21. H.H. Strehblow, and B. Titze, Corrosion Science, **17**, 461 (1977).
22. H.C. Man and D. R. Gabe, Corrosion Science, **21**, 713 (1981).
23. G.T Burstein and G. O. Ilevbare, in Corrosion Science, **38**, 2257 (1996).

Acknowledgements

Table 1. Chemical composition of Alloy 22 (UNS No. N06022) given in weight percent.

Element	Actual Composition			ASTM Requirements ASTM B575-Sheets
	Wrought	Welded (Weld/Filler Metal)	Welded (Base Metal)	
Mo	14.10	14.00	13.82	12.5-14.5
Cr	22.00	20.54	20.38	20.0-22.5
Fe	4.50	2.08	2.85	2.0-6.0
W	2.70	3.10	2.64	2.5-3.5
Co	1.30	0.03	0.01	0.0-2.5
C	0.003	0.004	0.005	0.000-0.015
Si	0.03	0.06	0.05	0.00-0.08
Mn	0.31	0.20	0.16	0.00-0.50
V	0.16	0.03	0.171	0.00-0.35
P	0.01	0.004	0.008	0.00-0.02
S	<0.01	0.001	0.0002	0.00-0.02
Ni	Bal.	Bal.	Bal	Bal.

Wrought Specimens from Heat # 2277-5-3203. Welded Specimens: Base metal from Heat #059902LL1; Weld/filler metal from Heat # XX1753BG.

Figure 1: Multiple Crevice Assembly (MCA), bottom. It shows the lollipop-like specimen (top), titanium grade two bolt (Teflon wrapped for electrical insulation), washers nut and ceramic washers.
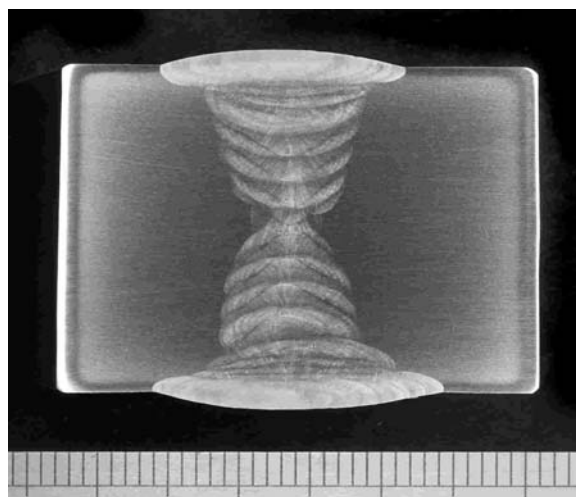

Figure 2. Cross-section of welded plate from which welded MCA samples were fabricated. Double-U weld was completed in 8-10 passes. The plate is 3.175 cm (1.25 inches) thick.
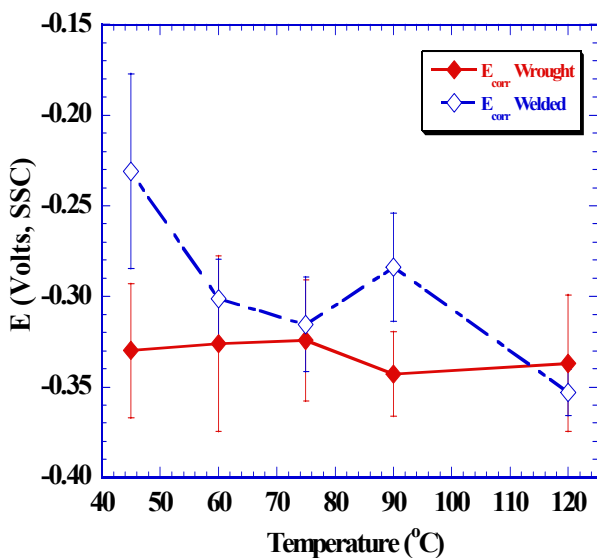

Figure 3. E_{corr} as a function of temperature on wrought and welded MCA samples in 5 M $CaCl_2$. E_{corr} was measured after 24 hour of immersion in solution.
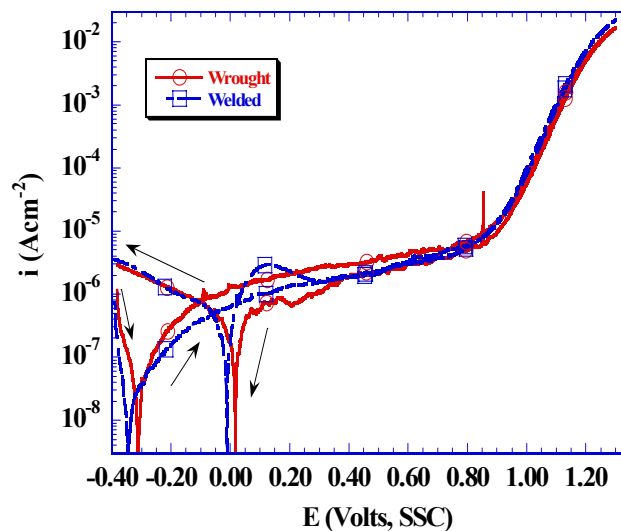
Figure 4: Polarization curves of wrought and welded MCA samples in 5 M $CaCl_2$ at 45 °C. Sweep rate, 0.1667mV/s
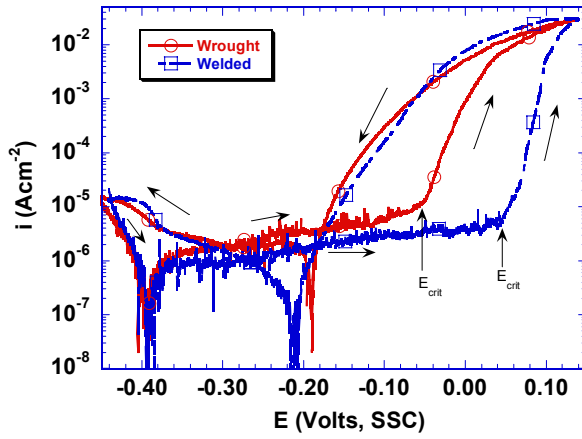
Figure 5: Polarization curves of wrought and welded MCA samples in 5 M CaCl$_2$ at 120 ^{o}C. Sweep rate, 0.1667mV/s
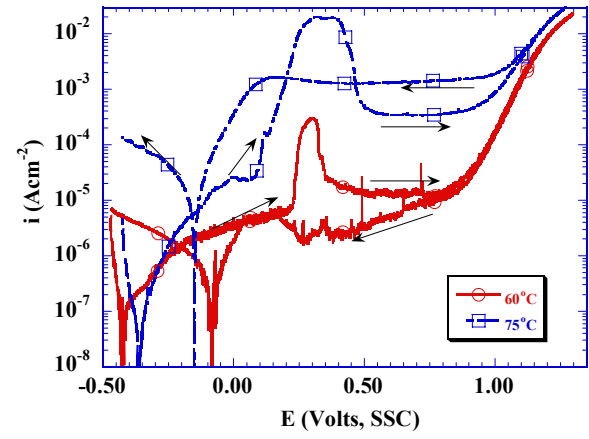
Figure 6: Polarization curves of wrought MCA samples in 5 M CaCl$_2$ at 60 and 75 ^{o}C. Sweep rate, 0.1667mV/s
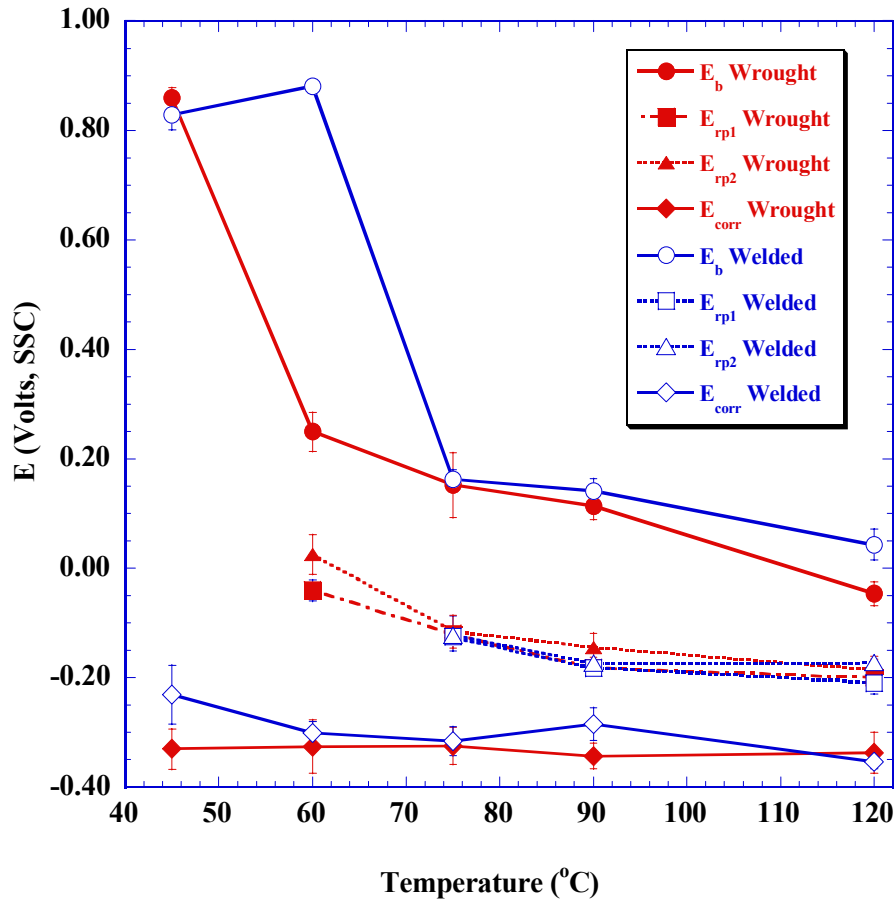

Figure 7. Average critical potential for breakdown, E$_b$, the repassivation potential E$_{rp}$, and the corrosion potential E$_{corr}$, as a function of temperature on wrought and welded MCA Alloy 22 samples in 5 M CaCl$_2$. E$_{rp1}$ is the potential at which the threshold current density of 1 x 10^{-6} Acm^{-2} was reached on the reverse sweep of the polarization curve. E$_{rp2}$ is the potential at which the reverse and forward sweeps of the polarization curve intersect.
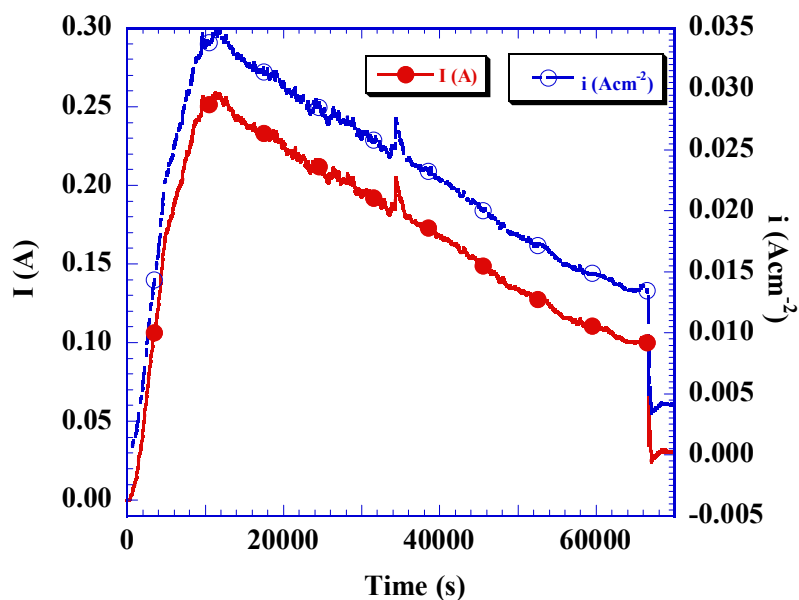
Figure 8. Current and current density transients of wrought MCA Alloy 22 at 0.325 V (SSC). These transients show 70 000s of the transient. The abrupt fall in current and current density at about 67 000s possibly coincides with the detachment of the lollipop head from the stem of the sample (refer to Figure 1).
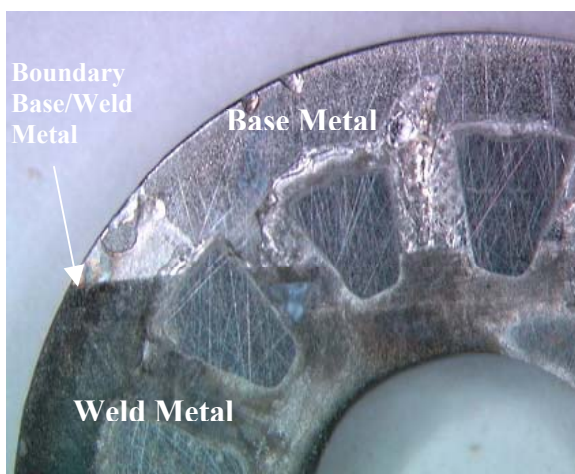

Figure 9. Welded MCA after 24 hours at E_{corr}, and cyclic polarization in 5 M $CaCl_2$ at 75 ^{o}C.
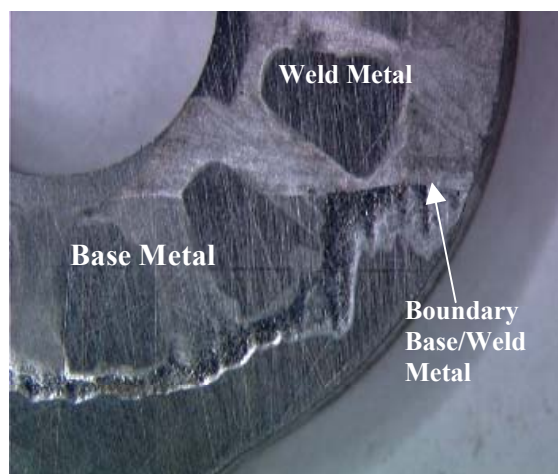

Figure 10. Welded MCA after 24 hours at E_{corr}, and cyclic polarization in 5 M $CaCl_2$ at 120 ^{o}C.